Materials Science and Engineering A 528 (2011) 4630–4642

Contents lists available at ScienceDirect

Materials Science and Engineering A

journal homepage: www.elsevier.com/locate/msea

Influence of intermetallic phases and Kirkendall-porosity on the mechanical properties of joints between steel and aluminium alloys

H. Springer[a], A. Kostka[a,*], J.F. dos Santos[b], D. Raabe[a]

[a] Max-Planck-Institut für Eisenforschung GmbH, 40237 Düsseldorf, Germany
[b] Helmholtz-Zentrum Geesthacht, Institute of Materials Research, Materials Mechanics, Solid-State Joining Processes, 21502 Geesthacht, Germany

ARTICLE INFO

Article history:
Received 10 December 2010
Received in revised form 16 February 2011
Accepted 17 February 2011
Available online 24 February 2011

Keywords:
Friction stir welding
Aluminium
Steel
Interdiffusion
Intermetallic phases

ABSTRACT

The formation of intermetallic reaction layers and their influence on mechanical properties was investigated in friction stir welded joints between a low C steel and both pure Al (99.5 wt.%) and Al–5 wt.% Si. Characterisation of the steel/Al interface, tensile tests and fractography analysis were performed on samples in the as-welded state and after annealing in the range of 200–600 °C for 9–64 min. Annealing was performed to obtain reaction layers of distinct thickness and composition. For both Al alloys, the reaction layers grew with parabolic kinetics with the η phase (Al_5Fe_2) as the dominant component after annealing at 450 °C and above. In joints with pure Al, the tensile strength is governed by the formation of Kirkendall-porosity at the reaction layer/Al interface. The tensile strength of joints with Al–5 wt.% Si is controlled by the thickness of the η phase (Al_5Fe_2) layer. The pre-deformation of the base materials, induced by the friction stir welding procedure, was found to have a pronounced effect on the composition and growth kinetics of the reaction layers.

© 2011 Elsevier B.V. All rights reserved.

1. Introduction

Dissimilar joining of iron (Fe) to aluminium (Al) alloys is of eminent technical interest, as it allows the use of these two essential engineering materials in the same design [1,2]. Thus, the high strength, good creep resistance, and formability of steels [3,4] may be combined with the low density, high thermal conductivity and good corrosion resistance of Al alloys [5,6] in one hybrid part. Applications for such dissimilar joints between Fe and Al alloys are ubiquitous and range from an improved strength-to-weight ratio in transportation systems [2] to high temperature corrosion protection in the chemical industry [7] or enhanced cooling efficiency for example in cryogenic technology [8].

Joining of Fe and Al alloys is impeded by the differences in their mechanical properties and melting temperatures and because of the formation of brittle intermetallic phases [9]. The Al–Fe phase diagram [10,11] shows three Al-rich intermetallic phases – ζ (Al_2Fe), η (Al_5Fe_2) and θ ($Al_{13}Fe_4$) – and the two ordered Fe-rich phases β′ (AlFe) and β″ ($AlFe_3$). Silicon (Si) plays an important role for the reactions and intermetallic phases when it is present in steel/Al alloy joints [12,13]. 11 ternary phases have been found, exhibiting relatively large and closely positioned homogeneity ranges. However, not all of those equilibrium phases necessarily form during joining or subsequent heat treatments [14,15].

Most previous experiments concerning interdiffusion between Fe or steel and Al alloys are concerned with phase identification and growth kinetics. The η phase was observed as the dominant reaction product at the interface between solid Fe and Al melts [16–18] with an additionally detected thin layer of θ between η and the solidified Al melt via selected area diffraction (SAD) in the transmission electron microscope (TEM) [19]. Interdiffusion experiments where both Al and Fe alloys remain in the solid state showed that the η phase retains as the major fraction of the developed reaction layer with a temperature dependent, parabolic growth rate [15,20,21]. The addition of Si to Al has been found to not only change the composition of the reaction layer but also to have a pronounced, temperature dependent effect on its growth kinetics compared to respective experiments with pure Al: numerous researchers described a deceleration of the reaction layer growth in interdiffusion experiments with Si containing Al melts [17,22–26]. However, an accelerated growth was observed for interdiffusion between low carbon (C) steel and an Al–Si alloy at 600 °C, below the melting temperature of Al [15].

The influence of intermetallic phases at the interface between steel and Al alloys on the mechanical properties of joints has been investigated for both solid state processes [27–29] and 'solid/liquid' joining procedures, where the Al base material is molten (welded) and the Fe or steel side of the joint remains solid (brazed) [30–32]. Achar et al. [30] studied the tensile strength of arc-welded

* Corresponding author at: Max-Planck-Institut für Eisenforschung GmbH, Mikrostrukturphysik und Umformtechnik, Max-Planck-Str. 1, D-40237 Düsseldorf, Germany. Fax: +49 211 6792 333.
E-mail address: a.kostka@mpie.de (A. Kostka).

0921-5093/$ – see front matter © 2011 Elsevier B.V. All rights reserved.
doi:10.1016/j.msea.2011.02.057

Ex. 2019
IPR2024-01376

(solid/liquid) joints after annealing at 150–450 °C for 1–100 h. With growing intermetallic layer thickness caused by the heat treatment, strongly decreasing joint strength was observed and the samples failed in the steel/Al interface region rather than the Al base material. The developed reaction layers exhibited a very complex build-up due to a bronze buffer layer on the steel sheet [30]. Agudo et al. [32] applied electron backscatter diffraction analysis (EBSD) in the scanning electron microscope (SEM) and analytical TEM to characterise the intermetallic phase layers formed in solid/liquid joints produced by a gas shielded metal arc welding process. It was shown that the build-up of the reaction layer was in reasonable agreement to those formed in interdiffusion experiments [31]. Other researchers [27,28] investigated steel/Al joints fabricated by solid-state friction welding, which typically results in much thinner reaction layers than solid/liquid interaction conditions. Mechsner and Klock [27] found that tensile samples annealed for 80 h at 350 °C and above no longer failed in the Al base material but they fractured brittle in the interface region. Along with the parallel decreasing strength of the joints, this behaviour was ascribed to nucleation and growth of intermetallic phases, but no effort was made to identify them [27]. Yilmaz et al. [28] tested steel/Al joints in which the reaction layer thickness was varied via differing welding parameters. The intermetallic phase present at the interface was claimed to be Al_3Fe (corresponds to the θ phase) based on energy dispersive X-ray (EDX) measurements, but no clear relation between reaction layer thickness and joint strength could be detected [28].

While the detrimental effect of growing reaction layers on the mechanical properties of steel/Al joints is well-known and the critical thickness for intermetallic reaction layers was found to be ~10 μm [30], only little information exists on the microstructural mechanisms governing this embrittlement-process.

2. Objective

The objective of the present work is to elicit the fundamental mechanisms how intermetallic reaction layers influence the mechanical properties of dissimilar joints between steel and Al alloys. Using samples of steel sheets pre-bonded by friction stir welding (FSW) to two different Al alloys (with and without Si), intermetallic layers of distinct thickness and composition were systematically produced by heat treatments, followed by tensile testing and interface characterisation. Additionally, the microstructural response of the friction-stirred base materials to the heat treatment and the growth kinetics of the intermetallic layers were investigated in these interdiffusion experiments starting with strongly pre-deformed base materials.

3. Materials and methods

Steel samples were cut from 2 mm thick sheets of unalloyed low C steel (0.12 wt.% C; European grade: DC01). Al samples were cut from 2 mm thick sheets of either commercially available Al of 99.5 wt.% purity (Al99.5) or Al containing 5 wt.% Si (AlSi5). The AlSi5 sheets were hot rolled at 450 °C to 2 mm thickness from cast blocks.

3.1. Production of samples

The specimen pairs (Al/steel, Al–Si/steel) were friction stir welded along their 300 mm base line (parallel to the rolling direction of the sheets) in a butt joint configuration at the Helmholtz-Zentrum Geesthacht, Germany. The following process parameters were applied: rotation speed, 400 rpm; travel speed, 5 mm s^{-1}; axial force, 10 kN. The tool had a shoulder diameter of 13 mm and a non-threaded, 2 mm long conical pin with a top diameter of 6.5 mm. The Al samples were placed at the retreating side and the steel samples on the advancing side of the rotating tool, while the bottom edge of the pin touched the bottom line of the steel sample.

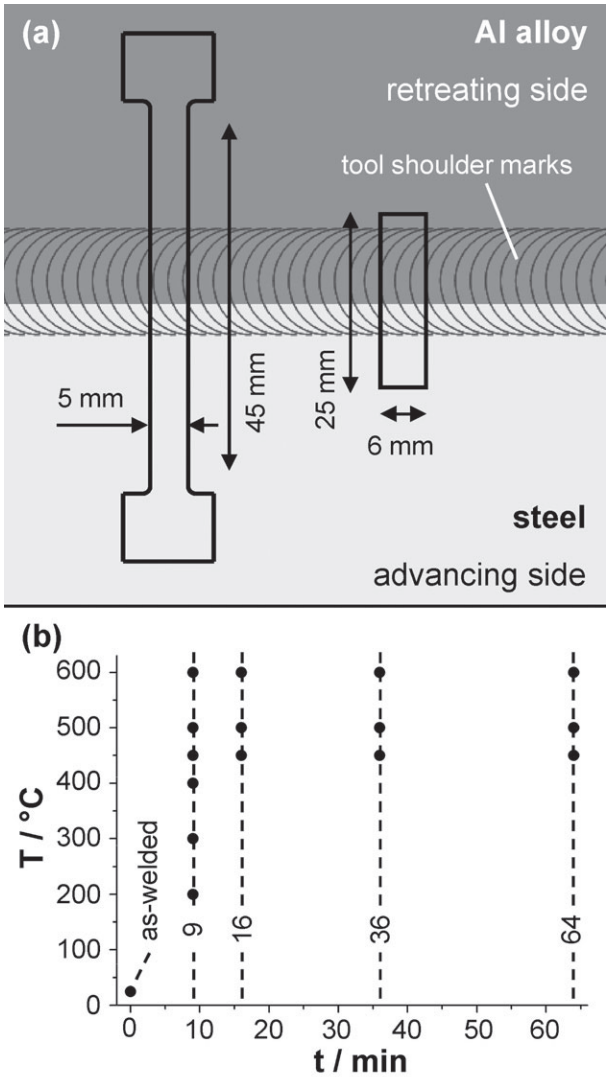

Fig. 1. Illustrations of the sample production process: (a) sketch of the friction-stir-welded base materials and the dimension and locations of samples for tensile testing (left) and interface characterisation (right). (b) Temperature/time matrix showing the different annealing treatments applied in this study.

From the bonded plates, samples for tensile testing and cross-sections for microstructural analysis were cut by spark erosion (Fig. 1(a)). For both types of joints, the samples were cut perpendicular to the welding direction and the steel/Al interfaces were positioned in the middle of the specimens. The cut samples were then annealed (air atmosphere) in the range of 200–600 °C for 9–64 min. Fig. 1(b) displays the different time (t)/temperature (T) settings applied in this study. Both Al alloys remain solid in the entire temperature range applied here; only at 600 °C the AlSi5 alloy consists of about 50% solid phase and 50% melt, according to the binary Al–Si phase diagram [33]. Despite being in this semi-solid, two phase state, the AlSi5 samples remain sufficiently viscous at 600 °C. Heating of the samples from room temperature to experimental temperatures took about 4 min; cooling was performed outside the furnace after the thermal exposure was complete.

Ex. 2019
IPR2024-01376

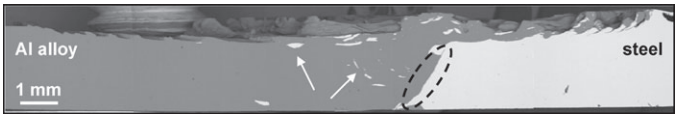

Fig. 2. Overview of the interfacial region between steel (right) and Al alloy (left) as a montage of SEM micrographs.

3.2. Characterisation

After annealing, the cross-sectional areas were prepared by grinding and polishing with standard metallographic techniques. The cross-sections were investigated using optical microscopy (OM), SEM, and TEM. Thicknesses of the reaction layers >1 μm were measured using a Leica DM4000M OM, which was equipped with an Image Access 9 image analysis system. Average values of reaction layer thicknesses were determined following same procedures as in [15,21,34]: the cross-sectional area of the reaction layer was measured over a distance of 150 μm; dividing this area by the length of the base line yielded the average thickness. For layers <1 μm this procedure could not be applied and respective values were obtained via SEM or TEM. SEM was performed using a Jeol JSM 6500F equipped with a field emission gun, an EDAX EDX system, and a TSL EBSD system [35]. TEM specimens were prepared from regions of interest along the steel/Al interface region using a Jeol JEM-9320 focused ion beam system (FIB) with a Ga^+ ion accelerating voltage of 30 kV. The TEM samples of about $25 \times 25 \times 0.1\ \mu m^3$ were prepared in such a way that the TEM foil normal laid parallel to the polishing plane. TEM was performed using a Jeol JEM-2200 FS operated at 200 kV for bright field (BF) and scanning-TEM (STEM) imaging, SAD and EDX chemical analysis. SAD patterns were indexed with the aid of the software package DDView 2004 (version 3.03) and the Powder Diffraction File PDF-2 (release 2004), both published by ICDD. The phases were identified according to the chemical and crystallographic information published elsewhere [13,15]. Images with a high atomic number contrast were acquired using a high angle annular dark field (HAADF) detector in STEM mode [36,37].

3.3. Tensile testing and fractography

Tensile tests were performed using a hydraulically operated testing machine Instron 8511. Three tensile tests with a speed of $10^{-4}\ s^{-1}$ were carried out at room temperature for each annealing T/t cycle; all values shown in this study represent the average of three measurements. Reference parameters for obtaining stress and strain values were the nominal cross-sectional area of $2 \times 5\ mm^2$ and the gauge length of 45 mm, respectively (Fig. 1(a)). After testing, the fracture surfaces were investigated using SEM and EDX analysis.

4. Results

4.1. Characterisation of the interface regions between steel and Al alloys

Fig. 2 shows an overview of the as-welded interface region between steel and Al alloy as a montage of SEM micrographs. On the top side of the cross-section, effects of the passing and rotating tool shoulder can be observed: Al was transported onto the steel surface and a slight groove remains in both base materials. The main inter-

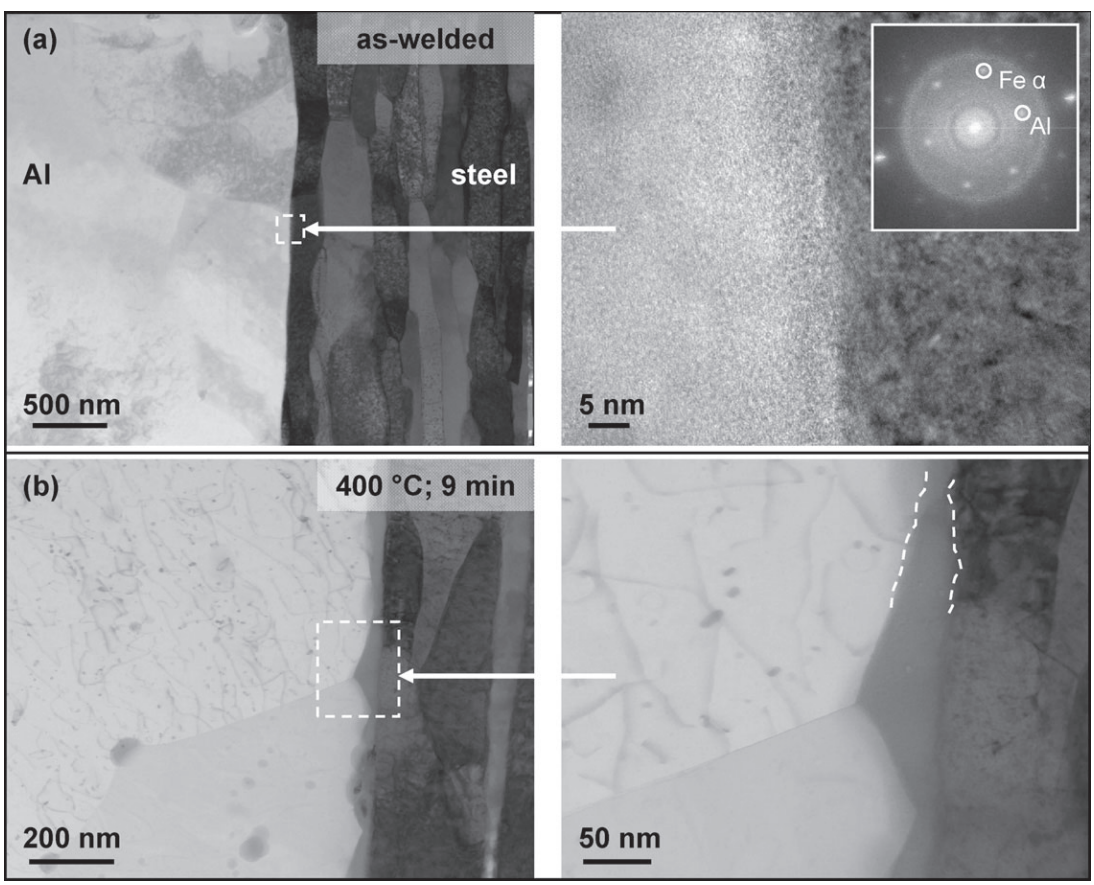

Fig. 3. TEM investigation of the interface region in joints between steel and Al99.5: (a) STEM BF micrograph from the as-welded state (left) and high resolution image with corresponding Fast-Fourier-Transformation (right) of the region highlighted on the left image. (b) STEM images after annealing at 400 °C for 9 min at different magnifications.

Ex. 2019
IPR2024-01376

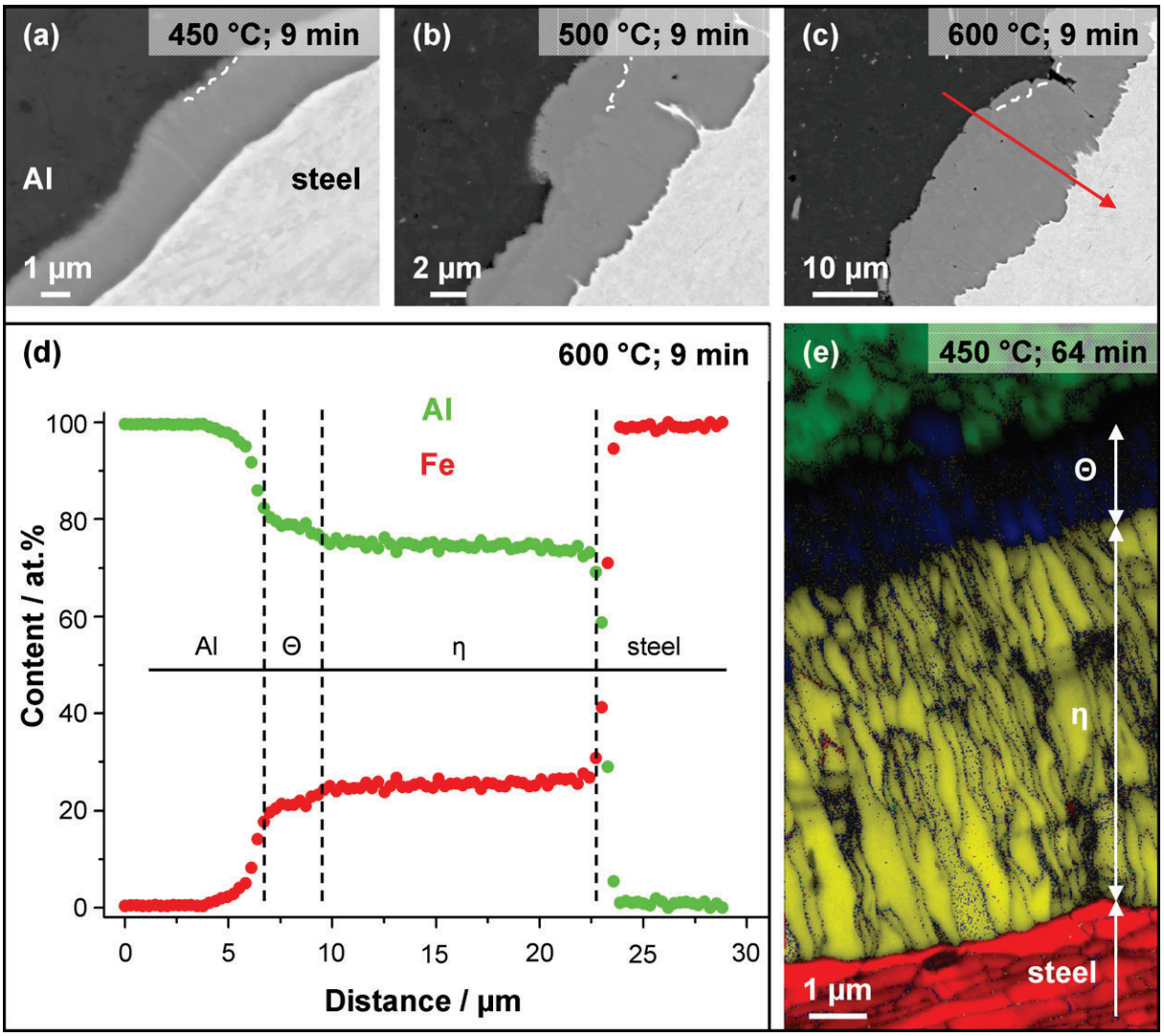

Fig. 4. Examples for SEM analysis of the reaction layers formed between steel and Al99.5: (a–c) SEM micrographs after annealing for 9 min at 450, 500 and 600 °C, respectively. (d) EDX line scan result obtained along the red arrow in (c). (e) Colour coded EBSD phase map after annealing at 450 °C for 64 min (Al – green, θ – blue, η – yellow, steel – red).

face between steel and Al alloy (highlighted by a black dashed oval in Fig. 2) is angled due to the conical shape of the tool pin. All further investigations concerning the interfacial reactions were conducted in this region of the samples. Additionally, detached steel particles can be observed in the Al side of the cross-section (marked by white arrows in Fig. 2) as a consequence of the complex material flow of the Al alloy during FSW [38]. Pores in the stir zone of the Al alloy (not shown here) rarely occurred on an irregular basis if the Al alloy failed to fully remerge after the tool had passed through.

4.1.1. Interface in joints with Al99.5

In the as welded state and in specimens annealed up to 400 °C, intermetallic reaction layers could not be observed in the SEM at the interface between Al99.5 and steel. Therefore, TEM samples were prepared from corresponding cross-sections (Fig. 3). Fig. 3(a) shows a STEM BF picture of the interface in the as-welded state (left side) and a high resolution TEM micrograph (right side) of the area highlighted on the left by a white dashed square. No intermetallic reaction layers can be observed at the interface. The Fast-Fourier-Transformation of the high resolution picture–shown as an insert on the right image in Fig. 3(a) – exhibits diffraction reflexes corresponding only to the base materials. Fig. 3(b) displays STEM BF micrographs of the interface after annealing at 400 °C for 9 min. A continuous reaction layer of about 50 nm thickness can be observed between Al and steel and is highlighted by white dashed lines in the image on the right, which corresponds to the white dashed square in the left image taken at lower magnification. Diffraction experiments in the TEM (not shown here) suggested that the reaction layer consists of the ζ phase.

After annealing at 450 °C and above, the reaction layers at the interface possessed a sufficient thickness for SEM analysis (>2 µm) and selected results are compiled in Fig. 4. Fig. 4(a–c) shows SEM micrographs of the reaction zones after annealing for 9 min at 450, 500 and 600 °C, respectively, at different magnifications. Two types of reaction layers with differing grey level can be observed and are highlighted by white dashed lines, namely, a lower layer adjacent to steel (down/right) and an upper layer adjacent to Al (top/left). The lower layer takes up the larger fraction of the reaction layer. With increasing annealing temperature the total thickness of the reaction layer grows from 1.9 µm at 450 °C to 13.6 µm at 600 °C. The reaction layers are continuous but vary in thickness along the interface. Additionally, the morphology of the interfaces towards the adjacent base materials changes with temperature: while the interface of the upper layer towards Al remains irregularly fringed on a

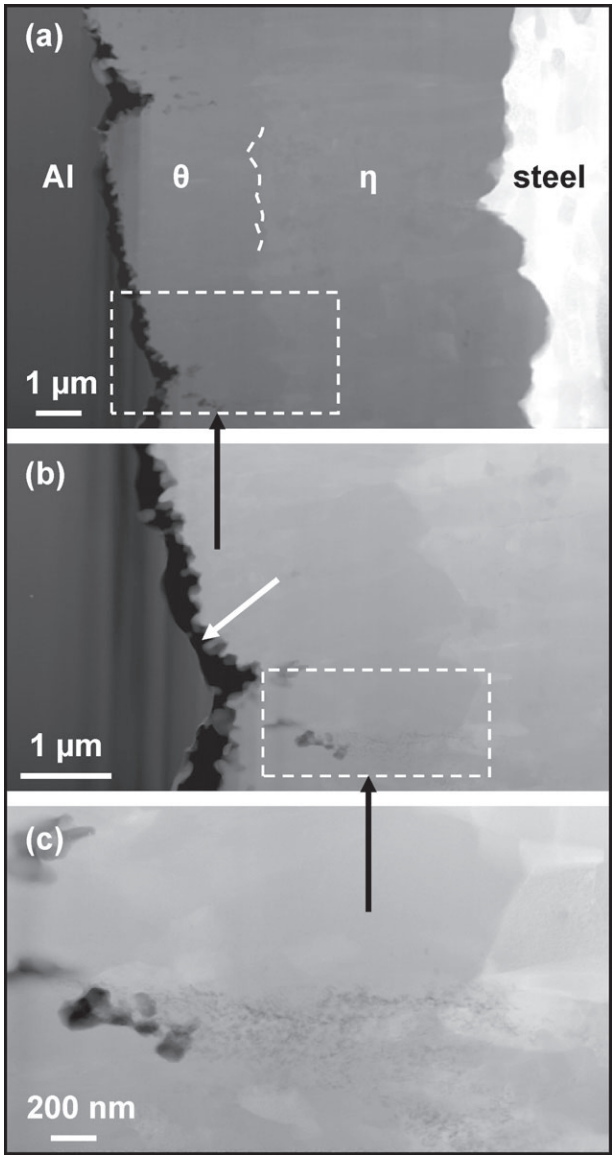

Fig. 5. STEM HAADF images taken at different magnifications, showing the reaction zone between steel and Al99.5 after annealing at 500 °C for 9 min.

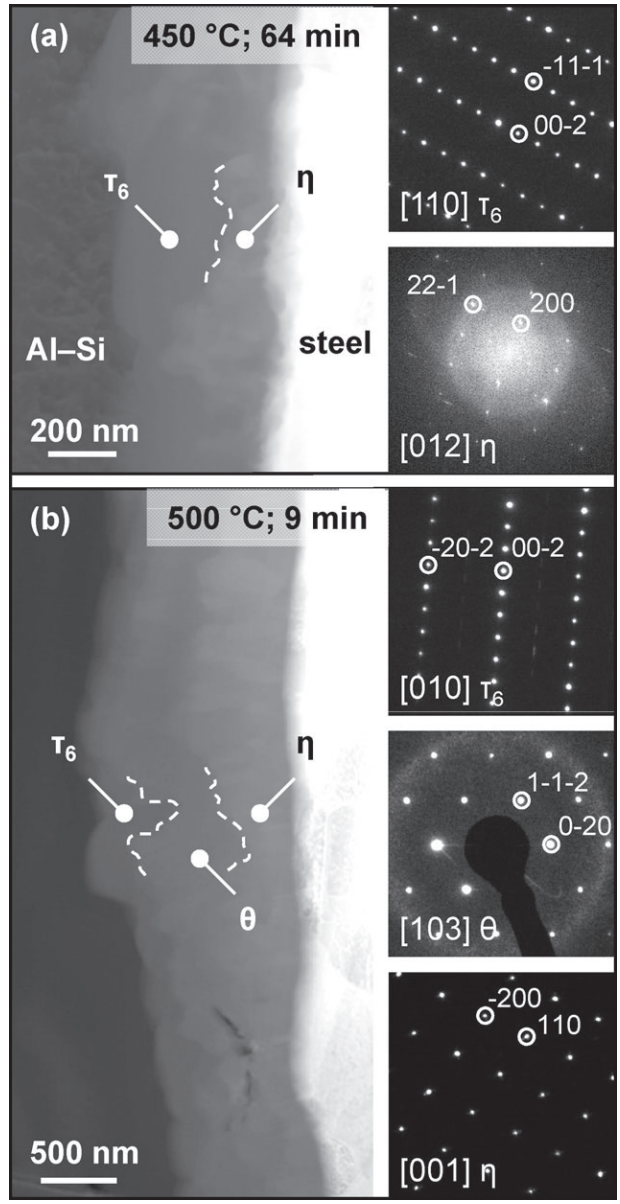

Fig. 6. TEM investigation of the interface region in joints between steel and AlSi5, showing STEM HAADF micrographs (left side) and SAD patterns of single phase regions (right side): (a) after annealing at 450 °C for 64 min. (b) After annealing at 500 °C for 9 min.

finer scale, the smooth interface at 450 °C between the lower layer and steel develops larger scale wavy features at 500 and 600 °C, as described in previous interdiffusion experiments [15,21]. The EDX line scan result (Fig. 4(d)) along the red arrow in Fig. 4(c) and the colour coded EBSD phase map (Fig. 4(e)) after annealing at 450 °C for 64 min allow to identify the two types of phases present in the reaction layers. The upper layer adjacent to Al consists of the θ phase (coloured blue in Fig. 4(e)), whereas the lower layer adjacent to steel is made up of η phase (yellow). Al and steel appear green and red in Fig. 4(e), respectively.

In order to confirm the SEM results and to investigate the reaction layers and their interfaces with higher resolution, TEM samples were prepared from a specimen annealed at 500 °C for 9 min. Fig. 5 shows STEM HAADF micrographs of increasing magnifications from top to bottom; the corresponding areas of the images are highlighted by white dashed rectangles. Diffraction experiments (not shown here) confirmed the phase sequence of Al–θ–η–steel obtained by SEM measurements (Fig. 4). A seam of interconnected pores can be observed at large fractions of the interface between Al and θ phase, as marked by the white arrow in Fig. 5(b). Fig. 5(c) shows pores of about 200 nm diameter in the θ phase region close to the partly disconnected Al/θ interface. Additionally, a trail of dark features leading to a pore through both η phase (right side) and θ phase (left side) can be observed; which seem to consist of nano-sized voids.

4.1.2. Interface in joints with AlSi5

In samples in the as-welded state and after annealing at up to 400 °C, the interface between AlSi5 and steel shows similar characteristics as in samples with Al99.5 (Section 4.1.1): TEM investigations revealed the absence of reaction layers in the as-welded state and discontinuous islands of intermetallic compounds of about 30 nm thickness after annealing at 400 °C for 9 min.

In contrast to experiments with Al99.5, even after annealing at 450 °C for up to 64 min and 500 °C for short annealing times, reaction layers remained so thin (<2 µm) to require characterisation using TEM (Fig. 6). Fig. 6(a) shows results from samples after

Ex. 2019
IPR2024-01376

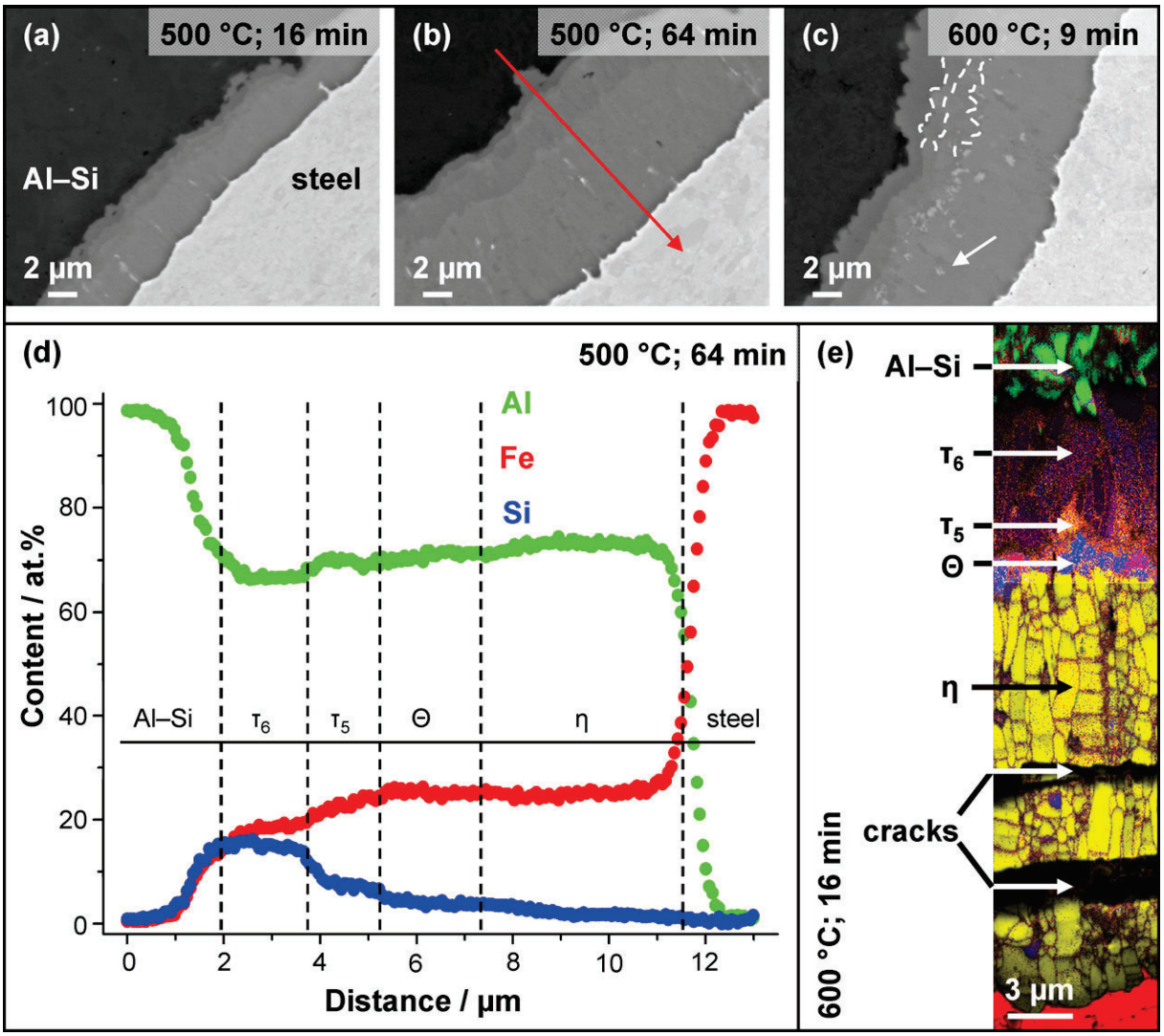

Fig. 7. Examples for SEM analysis of the reaction layers formed between steel and AlSi5: (a–c) SEM micrographs after annealing at 500 °C for 16 min, at 500 °C for 64 min and at 600 °C for 9 min, respectively. (d) EDX line scan result obtained along the red arrow in (b). (e) Colour coded EBSD phase map after annealing at 600 °C for 16 min (Al – green, τ_6 – violet, τ_5 – orange, θ – blue, η – yellow, steel – red).

annealing at 450 °C for 64 min. In the HAADF STEM micrograph (left side) two components in the now continuous reaction layer can be observed which differ in grey level. These two components were identified by SAD as τ_6 phase ($Al_{4.5}FeSi$) adjacent to the AlSi5 base material and η phase adjacent to steel. The respective locations of the two components are marked in the micrograph on the left side in Fig. 6(a); examples of indexed SAD patterns are given on the right side. TEM observations of samples after annealing at 500 °C for 9 min are displayed in Fig. 6(b). In the HAADF STEM micrograph on the left side, three components can now be differentiated. SAD (patterns given on the right side) identified the phases adjacent to the base material as τ_6 and η phase, the third component located between these two phases was identified as θ phase.

After annealing at 500 °C for more than 9 min and at 600 °C, the developed reaction layers reached thickness values allowing characterisation by SEM analysis; selected results are presented in Fig. 7. SEM micrographs of reaction zones after annealing at 500 and 600 °C for different times are shown in Fig. 7(a–c). Four reaction layers can be differentiated as highlighted by white dashed lines in Fig. 7(c). Towards the AlSi5 base material, three layers of varying but roughly equal thickness together take up about 1/3 of the entire layer. The 4th layer adjacent to steel accounts for the remaining 2/3 of the layer. While the interface of the reaction layer towards AlSi5 remains smoothly irregular with increasing layer thickness, the interface towards steel develops wavy features as observed in samples with Al99.5 (Fig. 4). From the EDX line scan result (Fig. 7(d)) along the red arrow in Fig. 7(b) and the colour coded EBSD phase map (Fig. 7(e)) after annealing at 600 °C for 16 min, the four types of phases present in the reaction layers can be identified. Directly adjacent to the AlSi5 base material is the τ_6 phase (violet coloured in Fig. 7(e)), followed by layers of τ_5 phase (Al_8Fe_2Si; orange) and θ phase (blue). The dominant component adjacent to steel is η phase (yellow). The white particles within η and at the interface between η and θ (marked with a white arrow in Fig. 7(c)) were found to be Si-rich; most probably consisting of the τ_1 phase ($Al_2Fe_3Si_3$) as shown in previous interdiffusion experiments [15,39].

4.2. Microstructure evolution of the Al-side

The applied heat treatment does not only result in interdiffusion and subsequent intermetallic phase formation at the steel/Al interface (Section 4.1), but is also expected to alter the microstructure of the base materials. The Al-side of samples in the as-welded state and after annealing for 9 min at 200, 400 and 600 °C was investi-

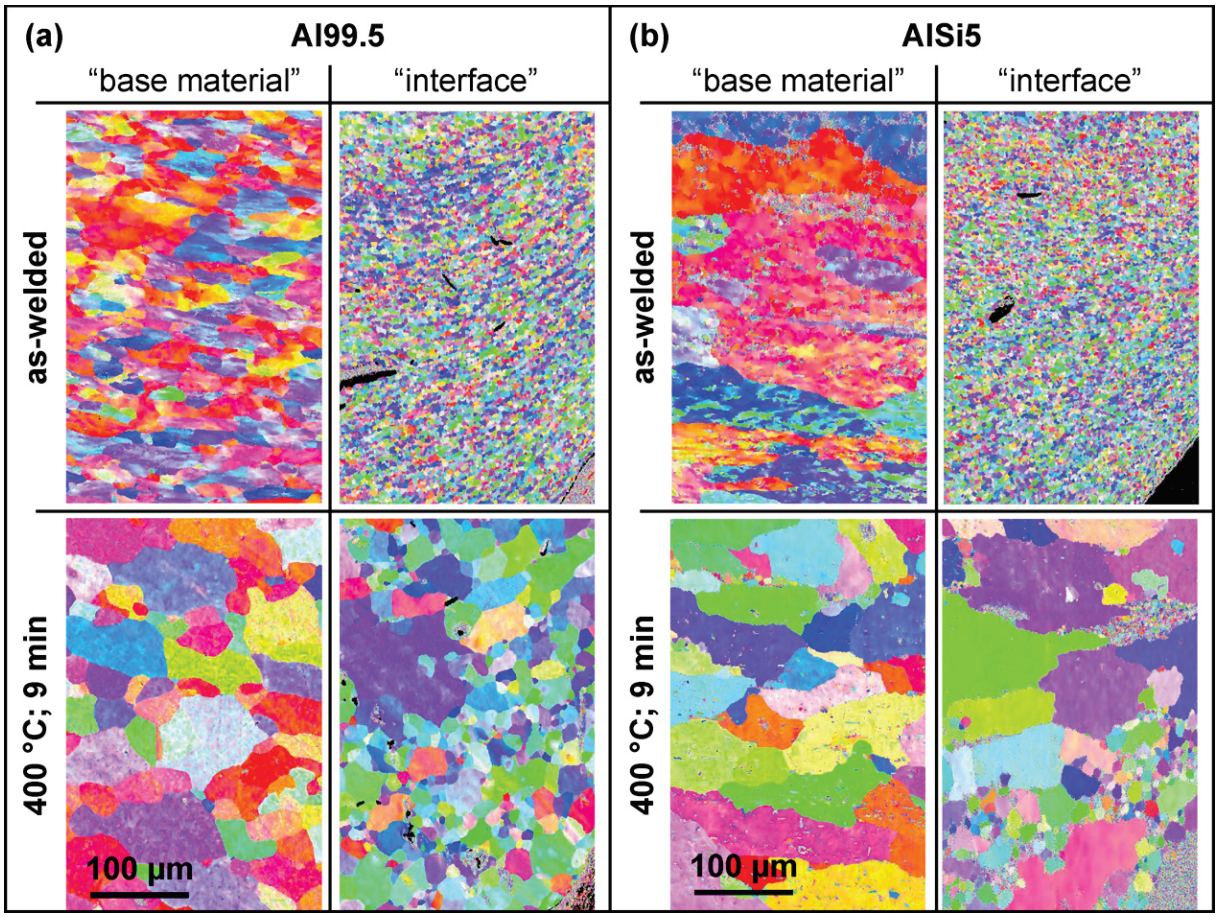

Fig. 8. Inverse pole figure maps obtained by EBSD analysis of the Al side of joints between steel and Al alloys: maps from the two scan locations in the as-welded state (top) and after annealing at 400 °C for 9 min (bottom) for joints with Al99.5 (a) and AlSi5 (b), respectively.

gated for both Al alloys. EBSD scans were performed for each sample both outside the weld region ("base material") and directly adjacent to the steel/Al interface ("interface"). Fig. 8(a) and (b) shows exemplary results as inverse pole figure maps from samples in the as-welded state (top) and after annealing at 400 °C (bottom) for samples with Al99.5 and AlSi5, respectively. Within the "interface" pictures, black and/or fine grained features within the Al alloy and at the bottom right edge represent steel particles and base material, improperly indexed by the chosen EBSD settings.

In the as-welded state, the Al99.5 base material exhibits an average grain size (AGS; approximate values) of 20 µm and the AlSi5 base material an AGS of 120 µm, while both alloys contain a considerable amount of low-angle grain boundaries (sub-grains) within laterally elongated grains. At the interface region, a much finer microstructure with an AGS of 3 µm can be observed in both alloys as a result of the severe plastic deformation induced by the FSW process [38]. Annealing at 200 °C (not shown in Fig. 8) left the grains size unchanged compared to the as-welded state.

After annealing at 400 °C the base material of both alloys exhibits an AGS of 35 µm each, a significantly reduced number of sub-grains and a more equiaxed microstructure. At the interface region, a bi-modal grain growth typical for secondary recrystallisation processes [40] can be observed for both Al alloys: while some grains remain at a size of 3 µm, others grow to 80 µm in diameter.

A further increase of the annealing temperature to 600 °C (not shown in Fig. 8) resulted in a slightly increasing AGS of the base materials with 40 µm for Al99.5 and 50 µm for AlSi5. The AGS at the interface region reached 30 µm for both alloys with a much more homogenous grain size distribution than as observed after annealing at 400 °C.

4.3. Growth of the intermetallic reaction layers at the interface between steel and Al alloys

The average thickness data (d in µm) from the annealing experiments at 450, 500 and 600 °C are presented in Fig. 9(a) and (b) as function of square root of time in min:

$$d = k \cdot \sqrt{t} \quad (1)$$

The thickness values from samples with Al99.5 are shown in Fig. 9(a) as circles and the values from samples with AlSi5 in Fig. 9(b) as squares. Empty symbols represent experiments at 450 °C, semi-filled symbols stand for 500 °C and solid filled symbols for 600 °C annealing temperature. No effort was made to measure the growth of the different components of the layers, but – as shown in Section 4.1 – the η phase takes up the largest fraction of the layers in this temperature range.

The growth rates (k in µm $s^{-1/2}$) derived from the kinetic data for samples with Al99.5 show similar values for all three temperatures: 0.176 for 450 °C, 0.141 for 500 °C and 0.242 for 600 °C. At 500 and even more pronounced at 450 °C, however, the deviation between the fitted line and the measured values is not as small as for the values obtained at 600 °C.

Results for samples with AlSi5 – plotted at a different scale in Fig. 9(b) – deviate significantly from the values measured in samples with Al99.5: at 450 °C, almost no growth of the reaction layer

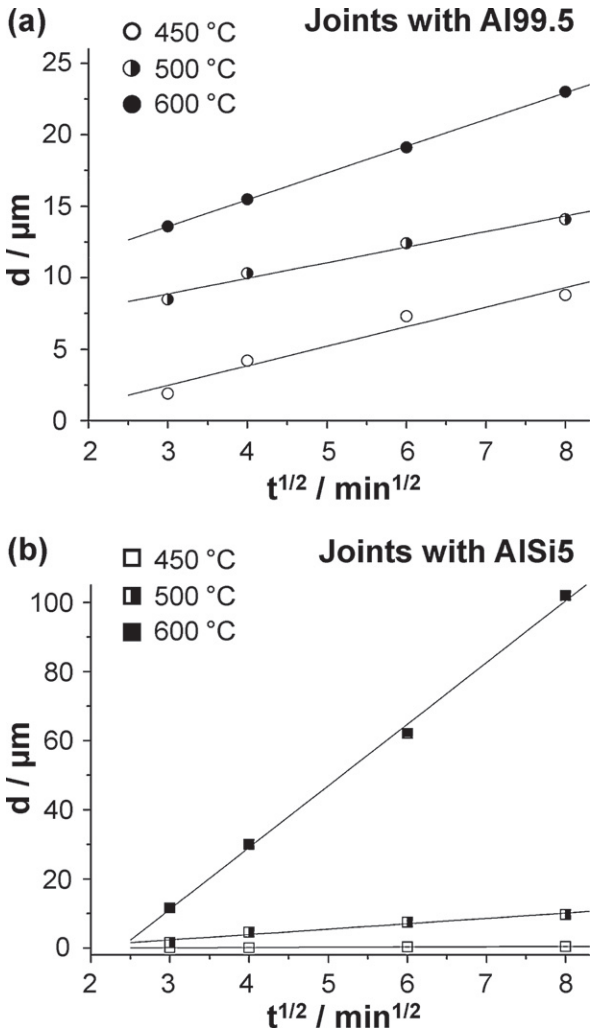

Fig. 9. Growth kinetics of the reaction layers formed between steel and Al alloys: (a) layer thickness as function of square root of time for joints with Al99.5. (b) Layer thickness in joints with AlSi5.

takes place, resulting in a rate of 0.01. While the k value of 0.201 for 500 °C is quite similar to the respective value shown Fig. 9(a), the growth rate at 600 °C is with a value of 2.303 almost 10 times larger than with Al99.5 at the same temperature.

4.4. Tensile testing of joints between steel and Al alloys

In order to have a reference point for the strength of the investigated joints, tensile tests were performed for all three base materials (not annealed). The samples were prepared as the tensile samples of the joints; i.e. perpendicular to the rolling direction of the sheets and having the same dimensions as sketched in Fig. 1(a). Fig. 10 shows typical stress/strain curves for the steel and both Al alloys. The steel exhibited a tensile strength R_m of 330 MPa and a fracture elongation ε_B of 28%. The Al alloys reached much lower respective values of 150 MPa/9.5% for AlSi5 and 120 MPa/6.5% for Al99.5.

4.4.1. Tensile testing of joints with Al99.5

The values of R_m, ε_B and the location of failure obtained for all tensile tests in joints with Al99.5 are listed in Table 1, together with the respective T/t cycle and the total reaction layer thickness d. The as-welded joints possess a tensile strength of 71.6 MPa (~60% efficiency compared to the Al99.5 base material). All samples from

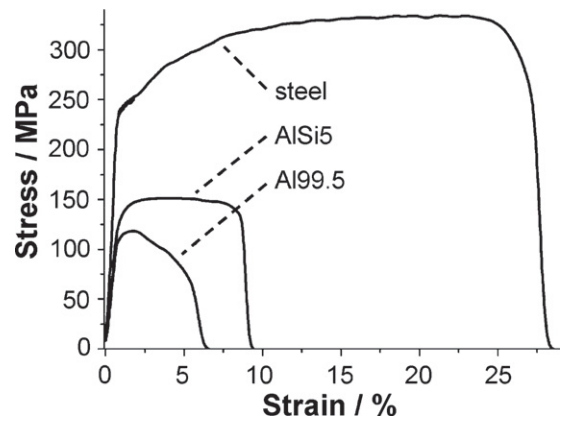

Fig. 10. Stress/strain curves from tensile tests of the three base materials from this study.

the as-welded state as well as after annealing at temperatures up to 450 °C failed in the Al weld region. In this temperature range R_m varies by about ±10 MPa due to minimal porosity in Al stir zone and slightly differing depth of the groove left by the passing welding tool shoulder (Section 4.1). After annealing at 300 °C, R_m of the joints drops to about 55 MPa and remains constant after annealing at 400 and 450 °C. The value of ε_B, however, increases from 3.6% in the as-welded state to values up to 9.3% after annealing between 200 and 450 °C. After annealing at 500 °C the samples begin to fail at the steel/Al interface. With reaction layer thickness growing above ~7 µm, R_m and ε_B of the joints drastically decrease. Samples annealed at 600 °C for 36 min or longer even failed during mounting in the testing machine. Fig. 11 shows typical results from SEM investigations of fracture surfaces of an interfacial failure in joints with Al99.5. Chemical compositions obtained from EDX measurements are included in the inserts taken at higher magnification, whose locations are highlighted by white dashed squares on the overview pictures of both Al side (Fig. 11(a)) and steel side (Fig. 11(b)) of the fracture surfaces. Three types of fractures can be differentiated: (1) bright, smooth cleavage surfaces with a chemical composition of 73 at.% Al and 27 at.% Fe on both sides, matching the composition of η and/or θ phase (Fig. 4(d)). (2) Fine grained, porous surfaces which appear bright on the steel side (73 at.% Al) and dark

Table 1
Reaction layer thickness d, ultimate tensile strength R_m, fracture elongation ε_B and the failure location of joints with Al99.5 together with the respective annealing parameters applied. The data represent average values from three tensile tests.

Joints with Al99.5					
T/°C	t/min	R_m/MPa	ε_B/%	d/µm	Failure in[a]
As-welded		71.6	3.6	0	a
200	9	74	4.2	<0.1[b]	a
300	9	55.6	5.1	<0.1[b]	a
400	9	56	9.3	0.05	a
450	9	55.8	7.9	1.9	a
450	16	53.7	6.9	4.2	a
450	36	53.3	7.5	7.3	a
450	64	44	5.9	8.8	a
500	9	48.3	4.3	8.5	b
500	16	44	2.5	10.3	a + b
500	36	34.3	1.9	12.4	a + b
500	64	27.3	0.9	14.1	b
600	9	14.6	1.2	13.6	b
600	16	2.7	0.8	15.5[c]	b
600	36	–b	–b	19.1[c]	–b
600	64	–b	–b	23[c]	–b

[a] a = Al-weld region; b = steel/Al interface.
[b] Not measured.
[c] Sample pre-fractured; a deviation of ±3 µm is possible.

Ex. 2019
IPR2024-01376

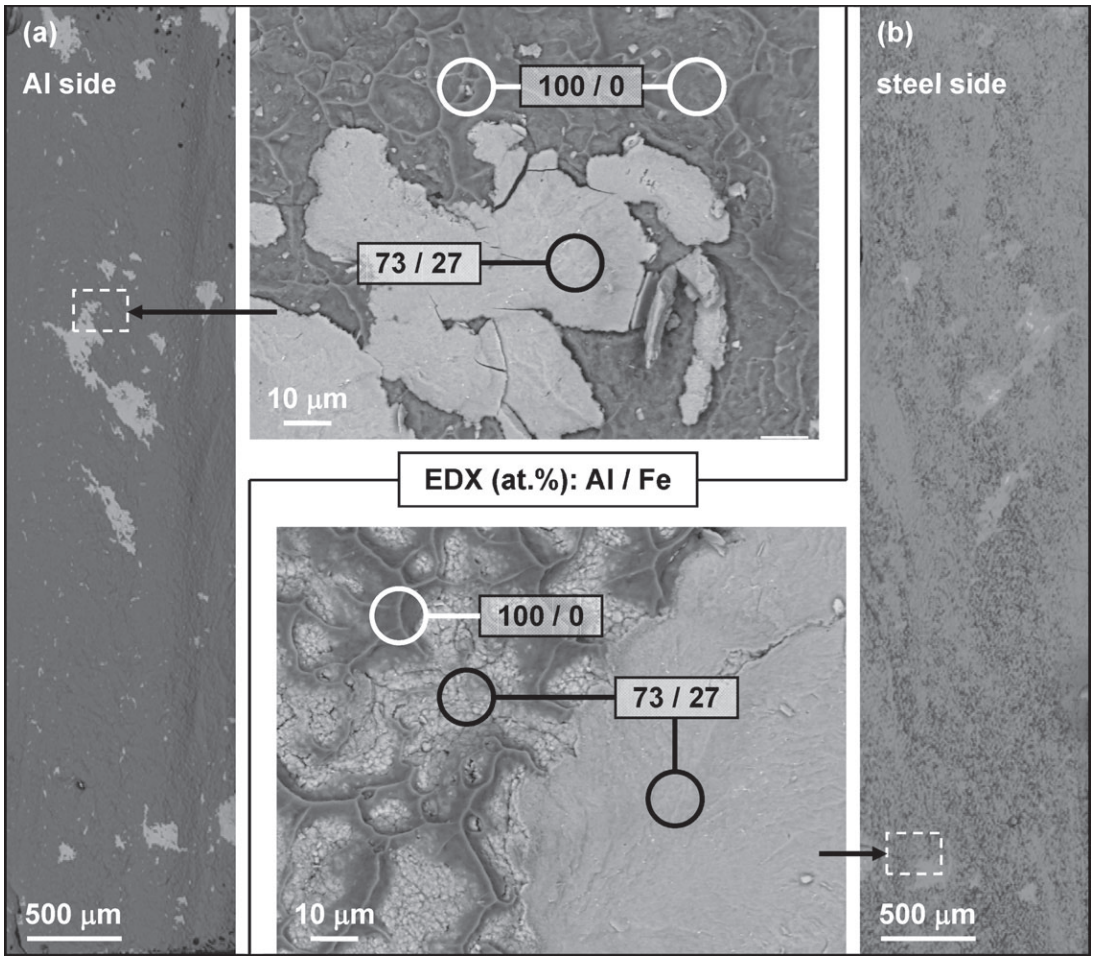

Fig. 11. SEM investigations of the fracture surfaces from a tensile test of a joint between steel and Al99.5 after annealing at 500 °C for 9 min. (a) Micrographs of the Al side. (b) Micrographs of the steel side. The pictures in the middle of this figure show details of the surfaces at higher magnification, as indicated by the respective white dashed squares on the outer pictures. Chemical concentrations of different features of the surfaces, as highlighted by circles on the respective micrographs, was measured by EDX (at.%).

on the Al side (100 at.% Al). (3) Dark ridges resembling ductile failure (100 at.% Al on both sides) located on the fine grained surface (2). Fracture types (2) and (3) take up the largest area fraction of the sample surfaces exhibiting interfacial failure. With increasing reaction layer thickness and subsequently decreasing joint strength, the quantity of ductile ridges (3) decreases until only the fine grained surfaces of type (2) prevail.

4.4.2. Tensile testing of joints with AlSi5

Table 2 lists the results of all tensile tests of joints with AlSi5, together with respective annealing parameters and reaction layer thickness. In the as-welded state and after annealing up to 450 °C, the results exhibit similar characteristics as for joints with Al99.5, only at a higher level of strength: R_m drops from 115 MPa in the as-welded state (77% efficiency) to ~100 MPa after annealing between 300 and 450 °C. Interfacial failure of joints sets in after annealing at 500 °C but at reaction layer thicknesses of just 1.6 μm. From there on, the ductility decreases with growing reaction layers to ~1% as with joints with Al99.5. The strength of joints, however, remains at a plateau of ~30 MPa. Fig. 12 displays fractography results for an interfacial failure in joints with AlSi5 (SEM and EDX analysis analogue as described in Fig. 11). The dominant fracture type observed on both steel and Al side is a smooth cleavage exhibiting an approximate chemical composition of 72 at.% Al, 26 at.% Fe and 2% Si, matching the composition of η phase (Fig. 7(d)). Very few dark, Al-rich ridges with ductile fracture behaviour appear on both surfaces. On the steel side, white Fe-rich areas (80–90 at.% Fe) can be observed, whose fraction decreases with increasing intermetallic layer thickness and declining joint strength.

Table 2
Reaction layer thickness d, ultimate tensile strength R_m, fracture elongation ε_B and the failure location of joints with AlSi5 together with the respective annealing parameters applied. The data represent average values from three tensile tests.

Joints with AlSi5					
T/°C	t/min	R_m/MPa	ε_B/%	d/nm	Failure in[a]
As-welded		115	4.4	0	a
200	9	115.3	5.3	<0.1[b]	a
300	9	103.3	5.2	<0.1[b]	a
400	9	108.6	9.6	0.03	a
450	9	90.6	4.2	0.12	a
450	16	103	5.9	0.1	a
450	36	98.3	5.2	0.33	a
450	64	97.3	5.6	0.47	a
500	9	100	3.7	1.6	a + b
500	16	102.6	5	4.6	a + b
500	36	78.3	2.1	7.5	b
500	64	69.3	1.9	9.7	b
600	9	41	1.6	11.6	b
600	16	30	1	30	b
600	36	–b	–b	62	–b
600	64	–b	–b	101.9	–b

[a] a = Al-weld region; b = steel/Al interface.
[b] Not measured.

Ex. 2019
IPR2024-01376

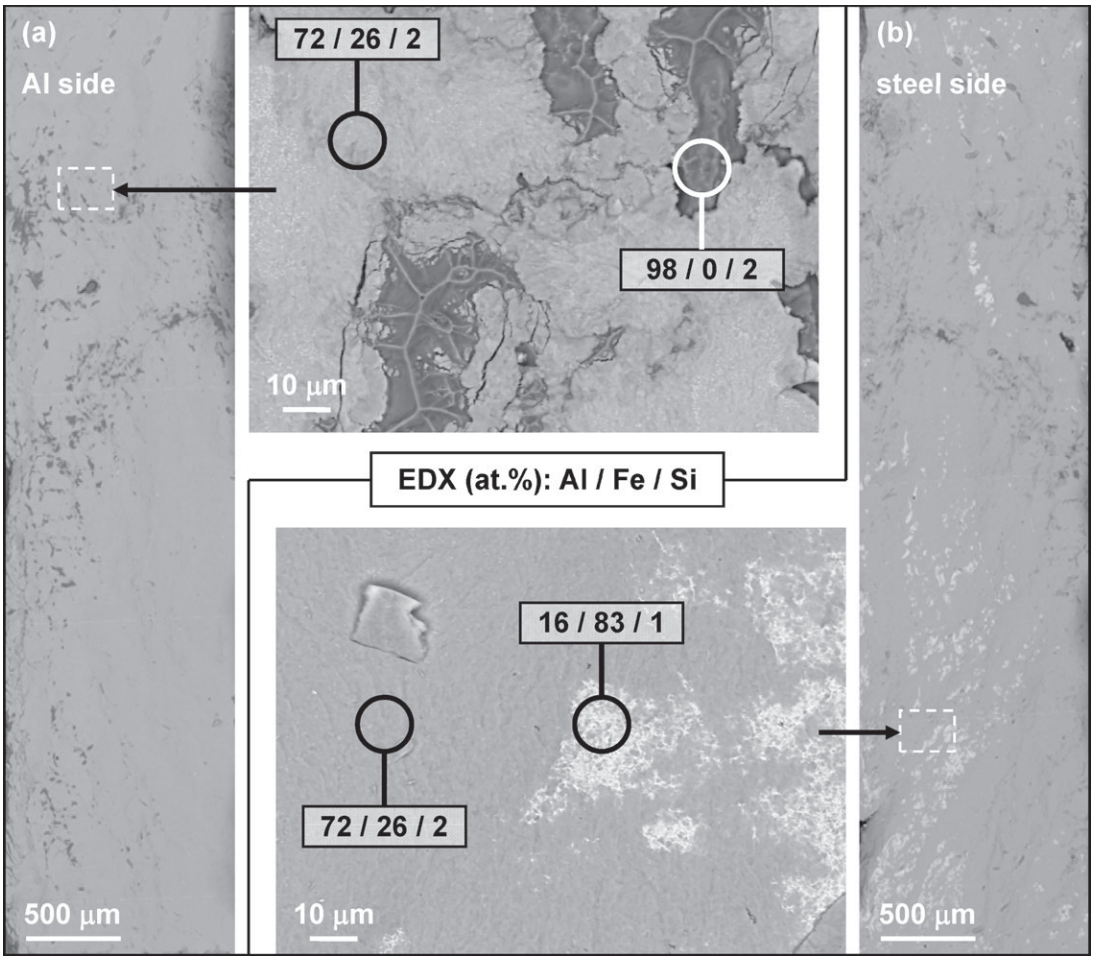

Fig. 12. SEM investigations of the fracture surfaces from a tensile test of a joint between steel and AlSi5 after annealing at 600 °C for 9 min. (a) Micrographs of the Al side. (b) Micrographs of the steel side. The pictures in the middle of this figure show details of the surfaces at higher magnification, as indicated by the respective white dashed squares on the outer pictures. Chemical concentrations of different features of the surfaces, as highlighted by circles on the respective micrographs, was measured by EDX (at.%).

5. Discussion

5.1. Formation of intermetallic reaction layers at the interface between steel and Al alloys

Despite the investigation of the steel/Al interface using high resolution techniques such as TEM, no intermetallic reaction layers could be detected in the as-welded state (Fig. 3(a)). Starting from this "direct bonding", reaction layer thicknesses >1 μm could be observed after annealing at 450 °C and above for joints with Al99.5 and of 500 °C for joints with AlSi5 (Section 4). In this temperature range, the η phase takes up the largest fraction of the total layer thickness for both Al alloys in agreement with previous results [15,21]. This prevalence of η was attributed to its rapid growth along its *c*-axis facilitated [18] by a highly open structural arrangement of atoms along this crystallographic direction [41].

After annealing in the range of 450–600 °C, the phase sequence of Al–θ–η–steel can be observed in joints with Al99.5 (Fig. 4). The appearance of θ between η and Al is contradictory to previous solid state interdiffusion experiments [15,21] and typical for the reaction of Fe alloys with Al melts [15,18,19,42]. This new result can be explained by the severe plastic deformation of the base materials induced by the FSW process prior to the heat treatment: the higher amount of stored energy available in the interdiffusion system of this study appears to facilitate nucleation and growth of the θ phase even at temperatures below the melting point of Al. This difference in nucleation conditions together with the comparably short annealing times chosen here might also explain the absence of thin bands of β′ and κ phase ($AlFe_3C$) between η and steel reported elsewhere [15].

The phases observed in joints with AlSi5 after annealing at 450 °C are τ_6 adjacent the Al–Si alloy and η towards steel. At 500 and 600 °C the phases θ and τ_5 appear in between τ_6 and η (Figs. 6 and 7). This time and temperature dependent composition of the reaction layers in joints with AlSi5 is expected in view of previous findings [15,39]. It is further noteworthy that the ternary eutectic phase τ_6 could be detected after annealing at 450 °C; much below the eutectic reaction temperature of 573 °C [12].

5.2. Growth kinetics of the reaction layers at the interface between steel and Al alloys

For both Al alloys the growth of the reaction layers can be approximated by parabolic rate laws in the range of 450–600 °C (Fig. 9(a) and (b)). The energy stored in the strongly deformed base materials does not only influence the composition of the reaction layers (as shown above) but also facilitates their growth [18]. Layer thicknesses which require hours to grow in diffusion bonding experiments [15,20,21] can be observed after only few minutes reaction time.

However, the energy available for intermetallic phase formation is also consumed by recrystallisation processes in the adjacent base

materials (Fig. 8), the amount of which depends on the annealing temperature. High temperatures apparently remediate the pre-deformation faster. Hence, for both Al alloys the best agreement of the kinetic data with a parabolic form (Eq. (1)) is obtained for annealing at 600 °C and the respective rate constants are in good agreement with previously published data [15]. The experiments of this study thus corroborate the strong acceleration of reaction layer growth for interdiffusion between steel and semi-solid AlSi5 at 600 °C compared to the reaction with pure Al [15]. The formation of θ phase in joints with Al99.5 apparently has no drastic effect on reaction layer growth. At lower temperatures (450 and 500 °C) the effect of deformation on layer growth becomes more apparent, especially for joints with Al99.5: the deviations between the values and the fitted line (Fig. 9(a)) indicate a slower growth rate for longer annealing times, following an accelerated growth at the beginning of the interdiffusion process. Thus, the calculated growth rates represent only an approximate value. The 'true' respective rate constants obtainable after longer thermal exposure are expected to be lower and to decrease with temperature. The same phenomenon applies for samples with AlSi5 after annealing at 500 °C, only the different scaling in Fig. 9(b) precludes its visibility. A direct comparison between the greatly differing growth rates for both alloys at 450 °C is difficult, as deformation of the base materials becomes increasingly important and both Al alloys might have reacted differently to the applied identical FSW parameters.

5.3. Relationship between interfacial microstructure and mechanical properties of the joints

In order to discuss the influence of intermetallic reaction layers on mechanical properties of the joints, R_m data for both Al alloys are plotted versus their respective d values in Fig. 13(a). Values from samples with Al99.5 are shown as circles and the values from samples with AlSi5 as squares. Empty symbols represent failure in the Al weld region and filled symbols stand for failure at the steel/Al interface. Semi-filled symbols indicate that both aforementioned failure locations could be observed. As some R_m/d values are very similar – especially for very thin reaction layers (<1 μm) – not all results listed in Tables 1 and 2 are shown in Fig. 13(a). Intermetallic phases themselves exhibit high hardness values and are inherently brittle [9], regardless of their dimensions. In the experimental conditions of this study, however, where the reaction layers are integral to a dissimilar joint, a strong effect of their thickness on joint strength can be observed. The deviant R_m/d sequences for both alloys – highlighted by dashed lines in Fig. 13(a) – allude to different mechanisms via which the growing reaction layers influence the joint strength.

Up to a layer thickness of ~7 μm, the joints with Al99.5 exhibit a constant strength of ~55 MPa while failing in the Al weld region. The drop to this value from the level of the as-welded state and the increasing ductility of respective joints (Table 1) can be explained by softening of the Al weld region due to recovery and recrystallisation processes, which occur parallel to growth of the reaction layers (Fig. 8). With layer thicknesses larger than 7 μm the strength drastically drops with the joints failing increasingly brittle at the steel/Al interface. A similar phenomenon has been described by Albright [43], who observed decreasing fracture toughness of Al/Fe deformation welds with increasing reaction layer thickness. Via X-ray diffraction measurements on fracture surfaces it was shown that the failure took place between the intermetallic reaction layer and the Al base material [43]. In accordance with crystallographic considerations and the findings of Heumann and Dittrich [18], this phenomenon was attributed to the formation of pores at the reaction layer/Al interface [43]. Following the scenario of Kirkendall and Smigelkas [44], such pores occur on the side of the faster diffusing element (Al in this case [45]), where vacancies, moving in the opposite direction of the dominant diffusive flux, condensate into voids. The results of this study suggest a similar behaviour: despite the well-known high hardness of the reaction layers compared to the adjacent base materials [9], joints with Al99.5 which exhibit interfacial failure ruptured mainly between the intermetallic phases and the Al base material, rather than within the reaction layer (Fig. 11). The topography of the respective fracture surfaces on steel and Al side does not fully match, similar as it was shown by Albright [43]. Additionally, the area fraction of the parallel observed ductile Al-ridges on both sides' decreases with declining joint strength (Fig. 11).

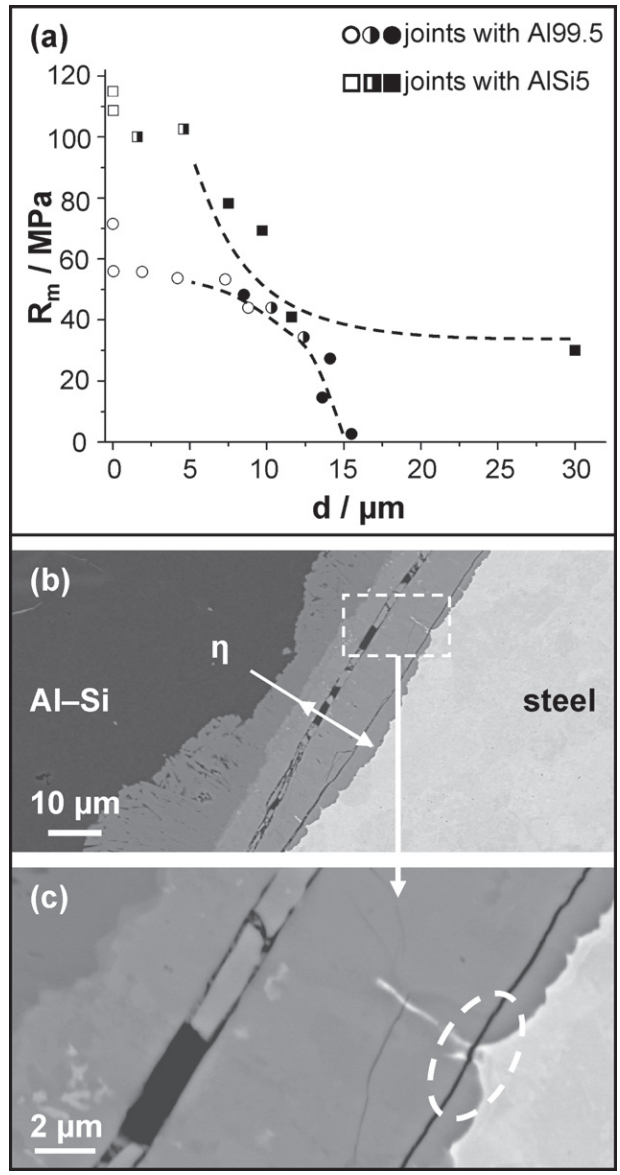

Fig. 13. (a) Plot of the tensile strength R_m of joints between steel and Al99.5 (circles) and AlSi5 (squares) versus the respective reaction layer thicknesses d (empty symbols – failure in the Al weld region, solid filled symbols – interfacial failure, semi-filled symbols – both interfacial and failure and in the Al weld region). (b and c) SEM micrographs of the reaction layer formed between steel and AlSi5 after annealing at 600 °C for 16 min at different magnifications. The sample fractured during metallographic preparation.

Thereby it can be concluded that the tensile strength of joints with Al99.5 is mainly governed by the formation of Kirkendall-porosity: growing intermetallic layers indirectly weaken the joint by an increasing formation of pores at the reaction layer/Al interface. Such a 'pseudo-embrittlement' (microscopic ductile

behaviour of the remaining Al-ridges while the entire joint fails at low strain) can also be observed in some Al alloys caused by 'precipitation-free-zones' along the grain boundaries [46]. The TEM results presented in Fig. 5 might indicate the evolution of the observed porosity (highlighted in Fig. 5(b)), as the trail of nano-sized voids shown in Fig. 5(c) could be linked to the above mentioned flux of vacancies.

While joints with AlSi5 also show a decrease in strength with increasing reaction layer thickness (Fig. 13(a)), remarkable differences compared to the respective data for joints with Al99.5 can be observed: the initial drop at low thickness values from the as-welded state is not as pronounced and failure at the steel/Al–Si interface sets in at much lower thickness values and at a higher level of strength. With further growing reaction layers the strength decreases until similar values are obtained as with Al99.5 (~40 MPa at 12 μm). From thereon, however, the strength of joints does not drop further but remains at about 30 MPa. The SEM investigations of respective fracture surfaces (Fig. 12) show that failure occurred mainly within the η phase as the dominant component of the reaction layer (Section 4.1.2). This more common behaviour (failure in η as the most brittle component [9]) is illustrated in Fig. 13(b) and (c), showing the cross-section of a joint annealed at 600 °C for 16 min at different magnifications. The SEM images correspond to the EBSD phase map shown in Fig. 7(e). The sample fractured within the η phase layer during metallographic preparation. It can be clearly seen that the crack propagating in the brittle intermetallic phase cuts through remains of steel at the irregular, wavy steel/η interface (marked by a white dashed oval in Fig. 13(c)) caused by the columnar η phase growth. These findings correspond to the detection of Fe-rich particles on the fracture surfaces (Fig. 12), whose area fraction decreases with growing reaction layers and declining joint strength.

Thus it can be concluded that the tensile strength of joints with AlSi5 is controlled by the thickness of the η phase layer: with increasing thickness the energy-consuming (and thus strength-preserving) crack-interception at the irregular η/steel interface becomes less frequent and the joint strength approaches the value of 25 MPa reported as the tensile strength of the η phase [9]. This corroborates the assumption of Achar et al. [30], who found a similar relation between strength and reaction layer thickness in their experiments. Moreover, the failure within the Al-weld region of joints with Al99.5 at thinner reaction layers (<7 μm) can now be explained: not enough pores have formed yet to promote interfacial separation and the Al base material is too soft compared to the stress required for η phase cleavage. The formation of Kirkendall-pores, on the other hand, does not seem to play a role in the investigated joints with AlSi5. This is in line with previous findings [15], where such pores have been observed – between the η phase and the interjacent phases towards the Al–Si alloy – only after longer annealing times (>8 h) and subsequently much thicker reaction layers (>150 μm) as applied/found in this study. Despite a possibly similar diffusive flux of vacancies, the different build-up of the reaction layer in joints with AlSi5 seems to have a strong effect on the formation of Kirkendall-porosity (nucleation conditions). The reason why the crack propagating through the η phase did not enter the adjacent intermetallic layers towards the Al–Si side of joints clearly requires further work, but it cannot be ruled out that the complex geometry of the steel/Al interface in the investigated of joints in this study (Fig. 2) also plays a role.

The fact that different failure mechanisms can be observed in joints with both Al alloys – despite the η phase as the dominant component in both cases–and that interfacial failure could be observed at much thinner reaction layers than the critical limit of ~10 μm given by Achar et al. [30], highlights the importance of taking the entire joint into account rather than focussing only on the thickness or hardness of the reaction layer: the build-up of the reaction layer and the constitution of interfaces and adjacent base materials just as well have an impact on the properties of dissimilar steel/Al joints.

6. Summary and conclusions

The present study investigated the formation of intermetallic reaction layers which form at the interface of FSW joints between low C (0.12 wt.% C) steel and both pure Al (99.5%) and Al–5 wt.% Si. Interface characterisation and tensile tests were performed with joints in the as-welded state and after annealing in the range of 200–600 °C for 9–64 min. From the obtained results the following conclusions can be drawn:

(1) In the as-welded state, no intermetallic reaction layers could be observed in TEM investigations. Layer thicknesses >1 μm formed during annealing at 450 °C and above in joints with Al99.5 and at 500 °C and above with Al–5 wt.% Si. In this temperature range, the η phase is the dominant component of the reaction layer for both Al alloys. Additionally, a layer of θ phase can be observed between η and the Al base material in joints with pure Al, which has been reported previously only for interdiffusion reactions of steels with Al melts. In joints with Al–5 wt.% Si, a time and temperature dependent build-up of the reaction layer could be observed. Annealing at 450 °C results in the appearance of the ternary eutectic phase τ_6 between the Al–Si alloy and η. At higher temperatures the phases θ and τ_5 form between τ_6 and η.
(2) At 600 °C, the growth of the reaction layers in joints with both Al alloys is in good agreement with a parabolic form and much thicker reaction layers can be observed with Al–5 wt.% Si compared to joints with pure Al. For temperatures below 600 °C our data suggest a faster growth at the beginning of the interdiffusion process. In general, similar reaction layer thicknesses as in conventional diffusion bonding experiments could be observed after much shorter annealing times.
(3) Both deviations in the phase sequence and a growth acceleration of reaction layers compared to previous interdiffusion experiments at similar temperatures can be explained by the higher amount of stored energy in the system investigated in this study, induced by the strong deformation of the base materials during FSW prior to the interdiffusion reactions.
(4) High resolution interface characterisation complimented with mechanical testing and fractography analysis allow explaining the role of intermetallic phases in joints between both Al alloys and steel: growing intermetallic layers indirectly weaken joints with pure Al by the formation of Kirkendall-porosity at the reaction layer/Al interface. Interfacial failure sets in at reaction layer thicknesses of ~7 μm and both strength and ductility of joints with pure Al drastically decreases. Interfacial failure in joints with Al–5 wt.% Si takes place as cleavage within the η phase; starting from reaction layer thicknesses of just 1.6 μm and at a higher level of strength than in joints with pure Al. The tensile strength of joints with Al–5 wt.% Si is governed by the thickness of the η phase. With growing η phase layers, the energy-consuming crack interception at the irregular η/steel interface becomes less frequent and the joint strength approaches the reported value for the tensile strength of the η phase. At reaction layer thicknesses below the starting of interfacial failure (temperatures of 200–450 °C), recovery and recrystallisation processes in the pre-deformed Al base materials controlled the strength of joints with both Al alloys.
(5) As an outlook, the strength of the bonding in interdiffusion reactions between steel and pure Al melts might be increased by a rapid transit from the melting temperature of Al (660 °C)

to about 400 °C during cooling of the joint from the reaction temperature. Thus, the formation of Kirkendall-porosity might be minimised and could be further reduced by a compressive loading of the joint during this temperature range of solid state interdiffusion.

Acknowledgements

The authors would like to acknowledge the support from the Virtual Institute for Improving Performance and Productivity of Integral Structures through Fundamental Understanding of Metallurgical Reactions in Metallic Joints (VI-IPSUS). The VI-IPSUS is an initiative of the Helmholtz Association coordinated by the Helmholtz-Zentrum Geesthacht.

References

[1] M.F. Ashby, Materials Selection in Mechanical Design, Butterworth-Heinemann, Burlington, MA, USA, 2005.
[2] U. Dilthey, L. Stein, Sci. Technol. Welding Joining 11 (2006) 135.
[3] R.W.K. Honeycombe, Steels – Microstructure and Properties, Arnold, London, 1981.
[4] W.C. Leslie, E. Hornbogen, in: R.W. Cahn, P. Haasen (Eds.), Physical Metallurgy, 4th Revised Edition, Elsevier Science, Amsterdam, 1996.
[5] D. Altenpohl, Aluminium Viewed from Within, Aluminium-Verlag, Düsseldorf, 1982.
[6] I.J. Polmear, Metallurgy of the Light Metals, Arnold, London, 1996.
[7] H. Hartwig, Aluminium 57 (1981) 615.
[8] S. Fukumoto, T. Inuki, H. Tsubakino, K. Okita, M. Aritoshi, T. Tomita, Mater. Sci. Technol. 13 (1997) 679.
[9] V.R. Ryabov, Aluminizing of Steel, Oxonian Press, New Delhi, 1985.
[10] O. Kubaschewski, Iron – Binary Phase Diagrams, Springer, Berlin, 1982.
[11] U.R. Kattner, Binary Alloy Phase Diagrams, ASM International, Materials Park, OH, USA, 1990, p. 147.
[12] G. Gosh, Ternary Alloys 5, VCH Verlagsgesellschaft, Weinheim, 1995, p. 394.
[13] N. Krendelsberger, F. Weitzer, J.C. Schuster, Metall. Mater. Trans. A 38 (2007) 1631.
[14] G.V. Kidson, J. Nucl. Mater. 3 (1961) 21.
[15] H. Springer, A. Kostka, E.J. Payton, D. Raabe, A. Kaysser-Pyzalla, G. Eggeler, Acta Mater. 59 (2010) 1586.
[16] W. Seith, C. Ochsenfarth, Z. Metall. 12 (1943) 242.
[17] E. Gebhardt, W. Obrowski, Z. Metall. 44 (1953) 154.
[18] T. Heumann, S. Dittrich, Z. Metall. 50 (1959) 617.
[19] G. Eggeler, H. Vogel, J. Freidrich, H. Kaesche, Prak. Metallogr. 22 (1985) 163.
[20] K. Shibata, S. Morozumi, S. Kosa, J. Jpn. Inst. Met. 30 (1966) 382.
[21] D. Naoi, M. Kajihara, Mater. Sci. Eng. A 459 (2007) 375.
[22] J.E. Nicholls, Corros. Technol. 11 (1964) 16.
[23] N. Komatsu, M. Nakamura, H. Fujita, J. Jpn. Inst. Light Met. 18 (1968) 467.
[24] A. Knauscher, Neue Hütte 19 (1974) 398.
[25] S.G. Denner, R.D. Jones, R.J. Thomas, J. Iron Steel Inst. 48 (1975) 241.
[26] G. Eggeler, W. Auer, H. Kaesche, J. Mater. Sci. 21 (1986) 3348.
[27] K. Mechsner, H. Klock, Aluminium 59 (1983) 850.
[28] M. Yilmaz, M. Cöl, M. Acet, Mater. Charact. 49 (2003) 421.
[29] A. Kobayashi, M. Machida, S. Hukaya, M. Suzuki, JSME Int. J. A 46 (2003) 452.
[30] D.R.G. Achar, J. Ruge, S. Sundaresan, Aluminium 56 (1980) 220.
[31] C.R. Radscheit Laserstrahlfügen von Aluminium mit Stahl. Ph.D. Thesis, Universität Bremen, Bremen, Germany, 1996.
[32] L. Agudo, D. Eyidi, C.H. Schmaranzer, E. Arenholz, N. Jank, J. Bruckner, A.R. Pyzalla, J. Mater. Sci. 42 (2007) 4205.
[33] J.L. Murray, A.J. McAllister, Bull. Alloy Phase Diagr. 5 (1984) 74.
[34] G. Eggeler, Ph.D. Thesis, Untersuchungen zum Feueraluminieren von niedriglegiertem Stahl, Friedrich Alexander Universität, Erlangen, 1985.
[35] A.J. Schwartz, M. Kumar, B.L. Adams (Eds.), Electron Backscatter Diffraction in Materials Science, Kluwer Academic, New York, 2000.
[36] N.D. Browning, M.F. Chisolm, S.J. Pennycook, Nature 366 (1993) 143.
[37] D.B. Williams, C.B. Carter, Transmission Electron Microscopy: A Textbook for Materials Science, Plenum Press, New York, 1996.
[38] R.S. Coelho, A. Kostka, J.F. dos Santos, A.R. Pyzalla, Adv. Eng. Mater. 10 (2008) 1127.
[39] T. Maitra, S.P. Gupta, Mater. Charact. 49 (2003) 293.
[40] G. Gottstein, Physical Foundations of Materials Science, Springer Verlag, Berlin, 2004.
[41] K. Schubert, U. Rosler, K. Anderko, L. Harle, Naturwiss 16 (1953) 437.
[42] A. Bouayad, C. Gerometta, A. Belkebir, A. Ambari, Mater. Sci. Eng. A 363 (2003) 53.
[43] C.E. Albright, Welding J., Res. Suppl. (1981) 207.
[44] A.D. Smigelkas, E.O. Kirkendall, Trans. AIME 171 (1947) 130.
[45] V.R. Ryabov, Welding of Aluminium Alloys to Steels, OPA Amsterdam B.V., Netherlands, 1998.
[46] Y.S. Sato, M. Urata, H. Kokawa, Met. Mater. Trans. A 33 (2002) 625.

Ex. 2019
IPR2024-01376